J|A|C|S ARTICLES

Published on Web 11/24/2010

Thermal Carbosilylation of Endohedral Dimetallofullerene $La_2@I_h$-C_{80} with Silirane

Michio Yamada,[†] Mari Minowa,[‡] Satoru Sato,[‡] Masahiro Kako,[§] Zdenek Slanina,[‡] Naomi Mizorogi,[‡] Takahiro Tsuchiya,[‡] Yutaka Maeda,[†] Shigeru Nagase,[||] and Takeshi Akasaka*[,‡]

Department of Chemistry, Tokyo Gakugei University, Koganei, Tokyo 184-8501, Japan, Center for Tsukuba Advanced Research Alliance, University of Tsukuba, Tsukuba, Ibaraki 305-8577, Japan, Department of Applied Physics and Chemistry, The University of Electro-Communications, Chofu 182-8585, Japan, and Department of Theoretical and Computational Molecular Science, Institute for Molecular Science, Okazaki, Aichi 444-8585, Japan

Received September 25, 2010; E-mail: akasaka@tara.tsukuba.ac.jp

Abstract: Thermal carbosilylation of endohedral dimetallofullerene $La_2@I_h$-C_{80} with silirane (silacyclopropane) is reported herein for the first time. Two diastereomers of the carbosilylated $La_2@I_h$-C_{80} have been isolated and characterized. The fascinating molecular structure of one diastereomer of the carbosilylated derivatives has been determined unambiguously using X-ray crystallographic analysis. Detailed characteristics of the molecular structures including their metal atom movements have also been revealed using NMR spectroscopic studies and computational calculations. Results revealed that two La atoms move dynamically inside the carbon sphere. Furthermore, electrochemical study has demonstrated that carbosilylation is effective to fine-tune the $La_2@I_h$-C_{80} electronic properties.

Introduction

Over the past two decades, fullerene chemistry has been explored widely because of their fascinating structures and properties.[1] The most pronounced feature of fullerenes is their high electron affinity, which is applicable to artificial photosynthesis[2] and organic electronics such as photovoltaics.[3] In view of raising the efficiency of organic devices of such kinds, exploration of functionalization methods of fullerenes is in great demand for achieving the desired electronic properties and functionalities. It is noteworthy that [6,6]-phenyl-C_{61}-butyric acid methyl ester ([60]PCBM)[4] is the most widely used fullerene derivative in the field of materials science; it has been used as an electron-accepting component in bulk-heterojunction (BHJ) solar cells. In that application, chemical functionalization of C_{60} is adopted to improve its solubility and miscibility.

Recently, encapsulation of metal atoms inside fullerene cages has been found to alter electronic properties of fullerenes greatly because electron transfer takes place from encaged metal atoms to carbon cages to stabilize them energetically.[5] Therefore, the encaged metal atoms are cationic, whereas the fullerene itself is anionic. Results show that the chemical reactivity of endohedral metallofullerenes also differs greatly from that of hollow fullerenes because of their unique electronic structures and enhanced electron affinity.[6] In fact, representative endohedral metallofullerenes, $M@C_{2v}$-C_{82} (M = La,[7] Ce,[8] Pr,[9] Gd,[10] and Y[7b]) and $M_2@I_h$-C_{80} (M = La[11] and Ce[12]), undergo both photochemical and thermal reactions with disiliranes (disilacyclopropanes) to form bis-silylated adducts, whereas bis-silylation

[†] Tokyo Gakugei University.
[‡] University of Tsukuba.
[§] The University of Electro-Communications.
[||] Institute for Molecular Science.

(1) For some books of fullerenes, see: (a) Hirsch, A. *The Chemistry of Fullerenes*; Thieme: Stuttgart, 1994. (b) Hirsch, A.; Brettreich, M. *Fullerenes - Chemistry and Reactions*; Wiley-VCH: Weinheim, 2004.
(2) (a) Kuciauskas, D.; Liddell, P. A.; Moore, A. L.; Moore, T. A.; Gust, D. *J. Am. Chem. Soc.* **1998**, *120*, 10880–10886. (b) Gust, D.; Moore, T. A.; Moore, A. L. *Acc. Chem. Res.* **2009**, *42*, 1890–1898.
(3) (a) *Fullerenes: From Synthesis to Optoelectronic Properties*; Guldi, D. M., Martín, N., Eds.; Kluwer Academic Publishers: Dordrecht, 2002. (b) Ros, R. B.; Cardona, C. M.; Guldi, D. M.; Sankaranarayanan, S. G.; Reese, M. O.; Kopidakis, N.; Peet, J.; Walker, B.; Bazan, G. C.; Van Keuren, E.; Holloway, B. C.; Drees, M. *Nat. Mater.* **2009**, *8*, 208–212.
(4) (a) Yu, G.; Gao, J.; Hummelen, J. C.; Wudl, F.; Heeger, A. J. *Science* **1995**, *270*, 1789–1791. (b) Rand, B. P.; Xue, J.; Uchida, S.; Forrest, S. R. *J. Appl. Phys.* **2005**, *98*, 124902. (c) Peet, J.; Heeger, A.; Bazan, G. C. *Acc. Chem. Res.* **2009**, *42*, 1700–1708.
(5) (a) *Endofullerenes: A New Family of Carbon Clusters*; Akasaka, T., Nagase, S., Eds.; Kluwer: Dordrecht, 2002. (b) Dunsch, L.; Yang, S. *Phys. Chem. Chem. Phys.* **2007**, *9*, 3067–3081. (c) Dunsch, L.; Yang, S. *Small* **2007**, *3*, 1298–1320. (d) Chaur, M. N.; Melin, F.; Ortiz, A. L.; Echegoyen, L. *Angew. Chem., Int. Ed.* **2009**, *48*, 7514–7538. (e) *Chemistry of Nanocarbons*; Akasaka, T., Wudl, F., Nagase, S., Eds.; Wiley-Blackwell: Oxford, 2010.
(6) Yamada, M.; Tsuchiya, T.; Akasaka, T.; Nagase, S. *Pure Appl. Chem.* **2010**, *82*, 757–767.
(7) (a) Akasaka, T.; Kato, T.; Kobayashi, K.; Nagase, S.; Yamamoto, K.; Funasaka, H.; Takahashi, T. *Nature* **1995**, *374*, 600–601. (b) Yamada, M.; Feng, L.; Wakahara, T.; Tsuchiya, T.; Maeda, Y.; Lian, Y.; Kako, M.; Akasaka, T.; Kato, T.; Kobayashi, K.; Nagase, S. *J. Phys. Chem. B* **2005**, *109*, 6049–6051.
(8) Wakahara, T.; Kobayashi, J.-i.; Yamada, M.; Maeda, Y.; Tsuchiya, T.; Okamura, M.; Akasaka, T.; Waelchli, M.; Kobayashi, K.; Nagase, S.; Kato, T.; Kako, M.; Yamamoto, K.; Kadish, K. M. *J. Am. Chem. Soc.* **2004**, *126*, 4883–4887.
(9) Akasaka, T.; Okubo, S.; Kondo, M.; Maeda, Y.; Wakahara, T.; Kato, T.; Suzuki, T.; Yamamoto, K.; Kobayashi, K.; Nagase, S. *Chem. Phys. Lett.* **2000**, *319*, 153–156.
(10) Akasaka, T.; Nagase, S.; Kobayashi, K.; Suzuki, T.; Kato, T.; Yamamoto, K.; Funasaka, H.; Takahashi, T. *J. Chem. Soc., Chem. Commun.* **1995**, 1343–1344.

of C_{60} proceeds only under photochemical conditions.[13] The high thermal reactivity of endohedral metallofullerenes with disilirane can be rationalized on the basis of their stronger electron acceptor property relative to C_{60} because the reactivity is strikingly distinctive of their first reduction potentials. It is also noteworthy that electronic properties of endohedral metallofullerenes can be tuned to a great degree by bis-silylation, which makes them much more electron-negative.[7b] In addition, results show that the three-dimensional movement of metal atoms in $M_2@I_h$-C_{80} can be converted to two-dimensional movement by bis-silylation onto the outer surface of $M_2@I_h$-C_{80} because the dynamic behavior of the cationic metal atoms is subject to the electrostatic potentials inside the cage.[11,12,14] In this context, controlling the movement and orientation of encaged species is expected to be valuable for the design of functional devices for molecular electronics on a nanoscale.[15] Therefore, introduction of silyl groups to endohedral metallofullerenes is an intriguing issue in terms not only of tuning the electronic properties of the molecules but also of controlling the metal atom movements. To date, various silylation using silicon compounds such as disiliranes,[14,16] disilanes,[17] silylenes,[18] and silyl anions[19] has been conducted to introduce silyl substituents into hollow fullerenes. Recent semiempirical calculations show that monosilylation of C_{60} is expected to increase the open circuit voltage up to 1 V in BHJ solar cells.[20] However, silylation of endohedral metallofullerenes has been limited to bis-silylation to date because of their distinct chemical reactivity from that of hollow fullerenes.[7b,8–12,21]

Among various silylations, carbosilylation is a useful synthetic strategy for introduction of silicon functionalities into carbon−carbon unsaturated bonds of organic molecules involving carbon−carbon bond formation.[22] Nevertheless, carbosilylation of alkenes has not been attained to date. Exploitation of carbosilylation of endohedral metallofullerenes is expected to provide not only fundamental aspects of chemical reactivity of anionic carbon spheres but also covalent derivatives bearing finely tuned electronic properties as candidates for future applications to organic molecular devices. Herein, we describe thermal carbosilylation of an endohedral dimetallofullerene, $La_2@I_h$-C_{80}, with silirane (silacyclopropane), for which no organometallic catalyst is required.

Experimental Section

General. All chemicals and solvents were purchased as reagent grade from Aldrich Chemical Co. Inc. and Wako Pure Chemical Industries Ltd. They were used as received. Toluene was freshly distilled over benzophenone sodium ketyl, CS_2 over P_2O_5 under dry N_2. 1,2-Dichlorobenzene (ODCB) was freshly distilled over P_2O_5 under vacuum. All reactions were performed in an inert atmosphere by application of a positive pressure of N_2. Preparative high-performance column chromatography (HPLC) was performed using chromatographs (LC-918 and LC-908; Japan Analytical Industry Co. Ltd.) that were monitored using UV absorption at 330 nm. The ^{1}H, ^{13}C, and ^{139}La NMR measurements were conducted on spectrometers (AVANCE 600, and 500; Bruker Analytik GmbH) with a CryoProbe system (Bruker Biospin K.K.). Mass spectrometry was performed (Bruker BIFLEX III; Bruker Daltonics Inc.) with 1,1,4,4-tetraphenyl-1,3-butadiene as the matrix. Vis−near-IR absorption spectra were measured using a spectrophotometer (UV-3150; Shimadzu Corp.). Cyclic voltammograms (CVs) and differential pulse voltammograms (DPVs) were recorded on an electrochemical analyzer (BAS CV50W; BAS Inc.). Platinum wires were used as the working and counter electrodes. The reference electrode was a saturated calomel reference electrode (SCE) filled with 0.1 M $(n\text{-Bu})_4NPF_6$ ($TBAPF_6$) in ODCB. All potentials are referenced to the ferrocene/ferrocenium couple (Fc/Fc^+) as the standard. The CVs were recorded using a scan rate of 20 mV s^{-1}. The DPVs were obtained using a pulse amplitude of 50 mV, pulse width of 50 ms, a pulse period of 200 ms, and a scan rate of 20 mV s^{-1}.

Preparation and Purification of $La_2@I_h$-C_{80}. Soot containing lanthanum metallofullerenes was prepared according to the reported procedure using a composite anode, which contains graphite and the lanthanum oxide with the atomic ratio of La/C equal to 2.0%.[23] The composite rod was subjected to an arc discharge as an anode under a 150 Torr He pressure. Raw soot containing lanthanum metallofullerenes was collected and extracted with 1,2,4-trichlorobenzene (TCB) solvent for 15 h. The soluble fraction was injected into the HPLC; a 5PYE column (20 mm × 250 mm i.d.; Cosmosil, Nacalai Tesque Inc.) was used in the first step and a Buckyprep column (20 mm × 250 mm i.d.; Cosmosil, Nacalai Tesque Inc.) in the second step to give pure $La_2@I_h$-C_{80}.

(11) Wakahara, T.; Yamada, M.; Takahashi, S.; Nakahodo, T.; Tsuchiya, T.; Maeda, Y.; Akasaka, T.; Kako, M.; Yoza, K.; Horn, E.; Mizorogi, N.; Nagase, S. *Chem. Commun.* **2007**, 2680–2682.

(12) Yamada, M.; Nakahodo, T.; Wakahara, T.; Tsuchiya, T.; Maeda, Y.; Akasaka, T.; Kako, M.; Yoza, K.; Horn, E.; Mizorogi, N.; Kobayashi, K.; Nagase, S. *J. Am. Chem. Soc.* **2005**, *127*, 14570–14571.

(13) Akasaka, T.; Ando, W.; Kobayashi, K.; Nagase, S. *J. Am. Chem. Soc.* **1993**, *115*, 10366–10367.

(14) (a) Yamada, M.; Wakahara, T.; Nakahodo, T.; Tsuchiya, T.; Maeda, Y.; Akasaka, T.; Yoza, K.; Horn, E.; Mizorogi, N.; Nagase, S. *J. Am. Chem. Soc.* **2006**, *128*, 1402–1403. (b) Yamada, M.; Someya, C.; Wakahara, T.; Tsuchiya, T.; Maeda, Y.; Akasaka, T.; Yoza, K.; Horn, E.; Liu, M. T. H.; Mizorogi, N.; Nagase, S. *J. Am. Chem. Soc.* **2008**, *130*, 1171–1176. (c) Yamada, M.; Okamura, M.; Sato, S.; Someya, C. I.; Mizorogi, N.; Tsuchiya, T.; Akasaka, T.; Kato, T.; Nagase, S. *Chem.-Eur. J.* **2009**, *15*, 10533–10542.

(15) Yamada, M.; Akasaka, T.; Nagase, S. *Acc. Chem. Res.* **2010**, *43*, 92–102.

(16) (a) Akasaka, T.; Mitsuhida, E.; Ando, W.; Kobayashi, K.; Nagase, S. *J. Am. Chem. Soc.* **1994**, *116*, 2627–2628. (b) Wakahara, T.; Han, A.; Maeda, Y.; Niino, Y.; Akasaka, T.; Yamamoto, K.; Kako, M.; Nakadaira, Y.; Kobayashi, K.; Nagase, S. *ITE Lett. Batteries, New Technol. Med.* **2001**, *2*, 649–653. (c) Han, A.; Wakahara, T.; Maeda, Y.; Niino, Y.; Akasaka, T.; Yamamoto, K.; Kako, M.; Nakadaira, Y.; Kobayashi, K.; Nagase, S. *Chem. Lett.* **2001**, 974–975. (d) Wakahara, T.; Han, A.; Niino, Y.; Maeda, Y.; Akasaka, T.; Suzuki, T.; Yamamoto, K.; Kako, M.; Nakadaira, Y.; Kobayashi, K.; Nagase, S. *J. Mater. Chem.* **2002**, *12*, 2061–2064.

(17) (a) Akasaka, T.; Suzuki, T.; Maeda, Y.; Ara, M.; Wakahara, T.; Kobayashi, K.; Nagase, S.; Kako, M.; Nakadaira, Y.; Fujitsuka, M.; Ito, O. *J. Org. Chem.* **1999**, *64*, 566–569. (b) Rahman, G. M. A.; Maeda, Y.; Wakahara, T.; Kako, M.; Sato, S.; Okamura, M.; Akasaka, T.; Kobayashi, K.; Nagase, S. *ITE Lett. Batteries, New Technol. Med.* **2003**, *4*, 60–66. (c) Maeda, Y.; Rahman, G. M. A.; Wakahara, T.; Kako, M.; Okamura, M.; Sato, S.; Akasaka, T.; Kobayashi, K.; Nagase, S. *J. Org. Chem.* **2003**, *68*, 6791–6794.

(18) (a) Akasaka, T.; Ando, W.; Kobayashi, K.; Nagase, S. *J. Am. Chem. Soc.* **1993**, *115*, 1605–1606. (b) Akasaka, T.; Mitsuhida, E.; Ando, W.; Kobayashi, K.; Nagase, S. *J. Chem. Soc., Chem. Commun.* **1995**, *15*, 1529–1530.

(19) (a) Kusukawa, T.; Ando, W. *Angew. Chem., Int. Ed. Engl.* **1996**, *35*, 1315–1317. (b) Kusukawa, T.; Ando, W. *J. Organomet. Chem.* **1998**, *561*, 109–120.

(20) Morvillo, P.; Bobeico, E. *Phys. Status Solidi RRL* **2008**, *2*, 260–262.

(21) (a) Akasaka, T.; Nagase, S.; Kobayashi, K.; Suzuki, T.; Kato, T.; Kikuchi, K.; Achiba, Y.; Yamamoto, K.; Funasaka, H.; Takahashi, T. *Angew. Chem., Int. Ed. Engl.* **1995**, *34*, 2139–2141. (b) Wakahara, T.; Sakuraba, A.; Iiduka, Y.; Okamura, M.; Tsuchiya, T.; Maeda, Y.; Akasaka, T.; Okubo, S.; Kato, T.; Kobayashi, K.; Nagase, S.; Kadish, K. M. *Chem. Phys. Lett.* **2004**, *398*, 553–556. (c) Iiduka, Y.; Ikenaga, O.; Sakuraba, A.; Wakahara, T.; Tsuchiya, T.; Maeda, Y.; Nakahodo, T.; Akasaka, T.; Kako, M.; Mizorogi, N.; Nagase, S. *J. Am. Chem. Soc.* **2005**, *127*, 9956–9957.

(22) Nii, S.; Terao, J.; Kambe, N. *J. Org. Chem.* **2000**, *65*, 5291–5297.

(23) Yamamoto, K.; Funasaka, T.; Takahashi, T.; Akasaka, T.; Suzuki, T.; Maruyama, Y. *J. Phys. Chem.* **1994**, *98*, 12831–12833.

Synthesis. 1,1-Bis(4-*tert*-butyl-2,6-dimethylphenyl)silirane (**1a**), (±)-2-(4-*tert*-butylphenyl)-1,1-bis(2,6-diethylphenyl)silirane ((±)-**1b**), and 1,1-(4-*tert*-butyl-2,6-dimethylphenyl)-2,2-diphenylsilirane (**1c**) were synthesized according to the literature.[24]

Carbosilylation of $La_2@I_h$-C_{80} with Silirane (±)-1b. A 30 mL aliquot of a toluene solution of $La_2@I_h$-C_{80} (1.0 mg, 8.1×10^{-4} mmol) and (±)-**1b** (2.7 mg, 5.9×10^{-3} mmol) was placed in a pyrex tube, degassed using freeze−pump−thaw cycles under reduced pressures, and then heated at 80 °C under the protection of Ar for 12 h. The solvent was removed using a rotary evaporator. The residue was dissolved in toluene and injected into an HPLC for analysis. Monoadduct mixture ((±)-**2-A** and (±)-**2-B**) and unreacted $La_2@I_h$-C_{80} were separated using HPLC with a Buckyprep-M (20 mm × 250 mm i.d.; Cosmosil; Nacalai Tesque Inc.) column with toluene at 9.9 mL min^{-1}. Monoadducts (±)-**2-A** and (±)-**2-B** were isolated by recycling HPLC procedure using a 5PYE column with toluene/*n*-hexane (1:1) at 9.9 mL min^{-1}. Yields: 46% ((±)-**2-A**) and 27% ((±)-**2-B**) (determined using HPLC).

Data for (±)-2-A. Dark brown solid. ^{1}H NMR (500 MHz, CS_2/CD_2Cl_2 (1:1), 293 K): δ 0.35 (t, ^3J = 7.2 Hz, 3H), 0.64 (t, ^3J = 7.4 Hz, 3H), 1.39 (t, ^3J = 7.4 Hz, 3H), 1.44 (s, 9H), 1.53 (t, ^3J = 7.5 Hz, 3H), 1.82 (dd, ^2J = 13.2 Hz, ^3J = 2.7 Hz, 1H), 2.72−2.86 (m, 4H), 3.04 (dd, ^3J = 14.1 Hz, ^2J = 13.2 Hz, 1H), 3.17−3.54 (m, 4H), 3.90 (dd, ^3J = 2.7 Hz, ^3J = 14.1 Hz, 1H), 6.91−7.65 (m, 10H). ^{13}C NMR (125 MHz, CS_2/CD_2Cl_2 (1:1), 293 K): δ 15.14 (i), 15.39 (i), 15.43 (i), 15.65 (i), 21.71 (h), 30.16 (j), 30.64 (j), 31.86 (a), 34.57 (j), 34.98 (b), 35.05 (j), 63.18 (g), 63.84 (o or p), 64.48 (o or p), 125.46 (m × 2), 125.85 (e × 2), 125.95 (d × 2), 126.39 (1C), 127.39 (m), 127.62 (m), 128.34 (1C), 129.50 (2C), 129.93 (2C), 130.24 (f), 131.03 (4C), 132.26 (1C), 132.61 (1C), 134.05 (1C), 134.49 (2C), 134.75 (k), 135.14 (1C), 135.17 (1C), 135.19 (1C), 135.23 (1C), 135.55 (1C), 136.34 (2C), 136.40 (1C), 136.56 (1C), 136.72 (1C), 136.97 (2C), 137.31 (1C), 137.40 (1C), 137.47 (1C), 137.50 (1C), 137.61 (1C), 137.76 (1C), 137.76 (1C), 137.80 (1C), 137.85 (1C), 138.71 (1C), 138.60 (1C), 138.75 (1C), 138.85 (1C), 138.97 (1C), 139.43 (1C), 139.62 (1C), 139.72 (1C), 139.98 (1C), 140.26 (1C), 140.51 (1C), 140.69 (1C), 140.75 (1C), 141.00 (1C), 141.18 (1C), 141.28 (1C), 141.87 (1C), 142.77 (1C), 142.96 (2C), 143.44 (1C), 144.75 (3C), 145.07 (2C), 145.83 (1C), 145.88 (1C), 145.96 (1C), 146.10 (1C), 146.46 (l), 147.52 (1C), 147.94 (l), 148.17 (k), 148.82 (1C), 148.96 (1C), 149.37 (1C), 149.46 (1C), 150.73 (1C), 150.79 (1C), 150.90 (1C), 153.81 (1C), 154.27 (1C). ^{139}La NMR (84.8 MHz, CS_2/CD_2Cl_2 (1:1) 278 K): δ 397.78 ppm. MALDI-TOF mass: *m*/*z* 1692 ($[M]^-$), 1238 ($[M - C_{32}H_{42}Si]^-$). Vis−near-IR (CS_2) λ_{max} 675 nm.

Crystal Data for (±)-2-A. $C_{118}H_{56}SiLa_2$, M_w = 1779.54, crystal size: 0.07 × 0.05 × 0.04 mm, monoclinic, $P2_1/n$, a = 14.097(6) Å, b = 14.762(7) Å, c = 34.122(14) Å, β = 90.415(7)°, V = 7100(5) Å^3, Z = 4, D_{calc} = 1.665 Mg/m^3, μ = 1.268 mm^{-1}, T = 90(2) K, 56 924 reflections, 9775 unique reflections; 3318 with $I > 2\sigma(I)$; R_1 = 0.1214 [$I > 2\sigma(I)$], wR_2 = 0.3680 (all data), GOF (on F^2) = 0.978. The maximum residual electron density is equal to 1.517 e Å^{-3}. All measurements were performed at beamline BL-8B of the Photon Factory, KEK, Japan. The data are obtainable free of charge from The Cambridge Crystallographic Data Centre via www.ccdc.cam.ac.uk/data_request/cif; CCDC 791725 ((±)-**2-A**) contains the supplementary crystallographic data used for this Article.

Data for (±)-2-B. Dark brown solid. ^{1}H NMR (500 MHz, CS_2/CD_2Cl_2 (1:1), 293 K): δ 0.35 (t, ^3J = 7.2 Hz, 3H), 0.58 (t, ^3J = 7.2 Hz, 3H), 1.36 (t, ^3J = 7.3 Hz, 3H), 1.37 (s, 9H), 1.72 (t, ^3J = 7.5 Hz, 3H), 1.87 (dd, ^2J = 12 Hz, ^3J = 1.8 Hz, 1H), 2.72−2.86 (m, 2H), 3.09 (dd, ^2J = 12 Hz, ^3J = 15 Hz, 1H), 2.96−3.27 (m, 4H), 3.46−3.62 (m, 2H), 3.86 (dd, ^3J = 1.8 Hz, ^3J = 15 Hz, 1H), 6.86−7.60 (m, 10H). ^{13}C NMR (125 MHz, CS_2/CD_2Cl_2 (1:1), 293 K): δ 14.70 (i), 15.74 (i), 15.85 (i), 16.65 (i), 26.34 (h), 30.39 (j × 2), 30.73 (b), 31.96 (a), 34.87 (j), 35.53 (j), 62.99 (o or p), 63.64 (g), 66.14 (o or p), 125.52 (1C), 125.56 (m × 2), 125.93 (1C), 126.38 (m), 127.31 (m), 128.06 (n), 128.89 (1C), 129.56 (2C), 130.09 (e × 2), 130.12 (1C), 130.65 (2C), 130.77 (d × 2), 134.94 (2C), 135.71 (2C), 136.12 (1C), 136.26 (1C), 136.34 (3C), 136.41 (1C), 136.50 (2C), 136.53 (1C), 136.61 (k), 136.71 (1C), 137.08 (1C), 137.18 (k), 137.21 (1C), 137.48 (1C), 137.59 (2C), 138.04 (1C), 138.12 (2C), 138.30 (2C), 138.33 (1C), 138.75 (1C), 138.98 (2C), 139.14 (1C), 139.21 (1C), 139.59 (1C), 139.74 (1C), 139.88 (1C), 140.36 (f), 141.10 (1C), 141.24 (1C), 141.33 (1C), 142.19 (2C), 142.21 (1C), 142.43 (1C), 142.99 (1C), 143.30 (1C), 143.98 (2C), 144.28 (1C), 144.31 (1C), 144.68 (1C), 144.86 (1C), 145.85 (1C), 145.94 (1C), 146.03 (1C), 146.66 (1C), 147.35 (1C), 147.38 (1C), 147.88 (1C), 148.24 (**l**), 149.35 (2C), 149.71 (**l**), 149.78 (1C), 149.90 (1C), 150.02 (1C), 150.27 (1C), 150.99 (1C). ^{139}La NMR (84.8 MHz, CS_2/CD_2Cl_2 (1:1) 278 K): δ −392.48 ppm. MALDI-TOF mass: *m*/*z* 1692 ($[M]^-$), 1238 ($[M - C_{32}H_{42}Si]^-$). Vis−near-IR (CS_2) λ_{max} 675 nm.

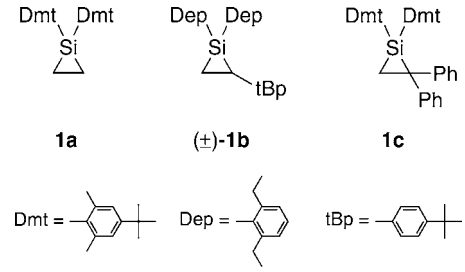

Figure 1. Structures of siliranes **1a**−**c**.

Theoretical Calculations. Geometries were optimized according to hybrid density functional theory (DFT) at the B3LYP[25] level using the Gaussian 03 program.[26] The effective core potential and the dz basis set[27] were used for La, only electrons in the outermost core orbitals were explicitly treated together with the valence electrons.[27] The contraction scheme used for the La basis set was (5s5p3d)/[4s4p3d] in standard notation. The split-valence d-polarized 6-31G*[28] basis set was used for H, C, and Si (the overall computational level is denoted as B3LYP/6-31G*∼dz).

Results and Discussion

Reactivity of $La_2@I_h$-C_{80} with Silirane. Siliranes are known to possess high reactivity toward nucleophilic reagents because of the strained and polar C−Si bonds in the silirane rings. To evaluate the reactivity of $La_2@I_h$-C_{80} toward siliranes, thermal and photochemical reactions were examined as an initial study. Siliranes of three kinds (**1a**−**c**) were subjected as the carbosilylation reagents, which possess variant substituents, as shown in Figure 1. Silirane **1a** has two 4-*tert*-butyl-2,6-dimethylphenyl (Dmt) substituents on the silicon atom, (±)-**1b** have two 2,6-diethylphenyl (Dep) substituents on the silicon atom and a 4-*tert*-butylphenyl (tBp) substituent on the vicinal carbon atom, and **1c** has two Dmt substituents on the silicon atom and two phenyl (Ph) substituents on the vicinal carbon atom. Because of their different substituents, **1a**−**c** exhibit distinct oxidation potentials. The first oxidation potentials of **1a**, (±)-**1b**, and **1c** are 1.17, 0.47, and 0.22 V, respectively, based on ferrocene/ferrocenium couple.[24] A toluene solution of $La_2@I_h$-C_{80} and an excess

(24) Nagatsuka, J.; Sugitani, S.; Kako, M.; Nakahodo, T.; Mizorogi, N.; Ishitsuka, M. O.; Maeda, Y.; Tsuchiya, T.; Akasaka, T.; Gao, X.; Nagase, S. *J. Am. Chem. Soc.* **2010**, *132*, 12106–12120.

(25) (a) Becke, A. D. *Phys. Rev. A* **1988**, *38*, 3098–3100. (b) Becke, A. D. *J. Chem. Phys.* **1993**, *98*, 5648–5652. (c) Lee, C.; Yang, W.; Parr, R. G. *Phys. Rev. B* **1988**, *37*, 785–789.

(26) Frisch, M. J.; et al. *Gaussian 03*, revision C.01; Gaussian, Inc.: Wallingford, CT, 2004.

(27) Hay, P. J.; Wadt, W. R. *J. Chem. Phys.* **1985**, *82*, 299–310.

(28) Hehre, W. J.; Ditchfield, R.; Pople, J. A. *J. Chem. Phys.* **1972**, *56*, 2257–2261.

Scheme 1

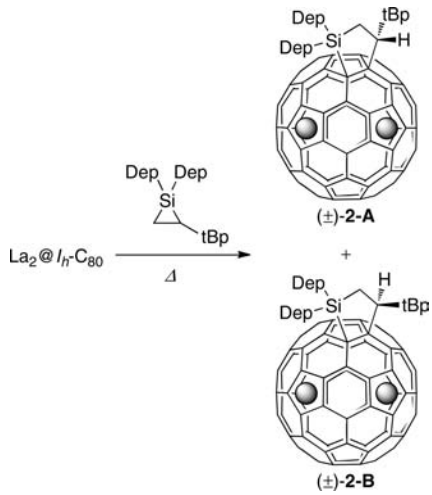

amount of silirane was photoirradiated with a halogen lamp (cut off <400 nm) for 1 h. After irradiation, the mixture was analyzed using analytical HPLC and matrix-assisted laser desorption ionization time-of-flight (MALDI-TOF) mass spectrometry. Regarding thermal reaction, a toluene solution of $La_2@I_h$-C_{80} and an excess amount of silirane was heated at 80 °C for 1 h; the mixture was analyzed as well. A new peak was observed in the HPLC profile of the thermal reaction mixture of $La_2@I_h$-C_{80} with (±)-**1b**; however, the other HPLC profiles were unchanged. The MALDI-TOF mass spectrum of the thermal reaction mixture of $La_2@I_h$-C_{80} with (±)-**1b** confirmed the formation of the 1:1 adduct, $La_2@I_h$-C_{80}[$SiDep_2(CH_2)CHtBp$]. Results clearly demonstrate that (±)-**1b** reacts smoothly with $La_2@I_h$-C_{80} thermally to form the corresponding monoadduct, although **1a** and **1c** do not. Recently, we found that reaction of C_{60} with (±)-**1b** proceeds only under photochemical conditions in which the reaction involves electron-transfer process from silirane to $^3C_{60}$*.[24] The high thermal reactivity of $La_2@I_h$-C_{80} toward (±)-**1b** can be rationalized on the basis of its stronger electron-accepting property relative to C_{60}. Therefore, it is reasonable to consider that the thermal reaction of $La_2@I_h$-C_{80} with (±)-**1b** proceeds via electron-transfer as well. In fact, silirane **1a**, having the highest oxidation potential, does not react with $La_2@I_h$-C_{80} under either thermal or photochemical conditions. However, the inert reactivity of **1c** is possibly caused by steric hindrance around the C−Si bond.

Synthesis and Characterization of Carbosilylated $La_2@I_h$-C_{80}. To characterize the reaction products, a substantial amount of the carbosilylated $La_2@I_h$-C_{80} was synthesized by the thermal reaction of $La_2@I_h$-C_{80} with (±)-**1b**, as shown in Scheme 1. An HPLC analysis showed that the reaction mixture contains two diastereomers of the monoadducts. Preparative HPLC techniques, involving recycling procedure using a 5PYE column, afforded isolation of the two diastereomers, (±)-**2-A** and (±)-**2-B**, in a ratio of 2:1. The MALDI-TOF mass spectra of (±)-**2-A** and (±)-**2-B** ($C_{112}H_{42}La_2Si$) under negative ionization conditions both show strong M^- peaks at *m*/*z* 1692 and fragment peaks of the parent cage $La_2@I_h$-C_{80} at *m*/*z* 1238.

Figure 2 depicts the vis−near-IR absorption spectra of (±)-**2-A**,**B**, in which those of $La_2@I_h$-C_{80}, (±)-1,4-$La_2@I_h$-$C_{80}(Dep_2Si)_2CH_2$ ((±)-**3**),[11] [5,6]-$La_2@I_h$-$C_{80}(CH_2)_2NTrt$ (Trt = trityl) (**4**),[14c] and [6,6]-$La_2@I_h$-$C_{80}(CH_2)_2NTrt$ (**5**)[14a,c] are also given. In bis-silylated $La_2@I_h$-C_{80} derivative (±)-**3**, the two silicon atoms are bonded to carbon atoms at 1,4-position on

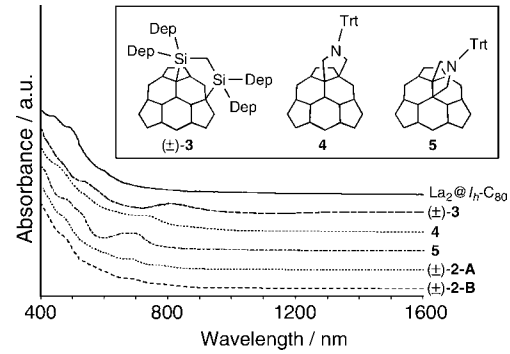

Figure 2. Vis−near-IR absorption spectra of (±)-**2-A** and (±)-**2-B**, in which those of $La_2@I_h$-C_{80}, (±)-**3**, **4**, and **5** are also given. The inset shows partial structures of (±)-**3**, **4**, and **5**.

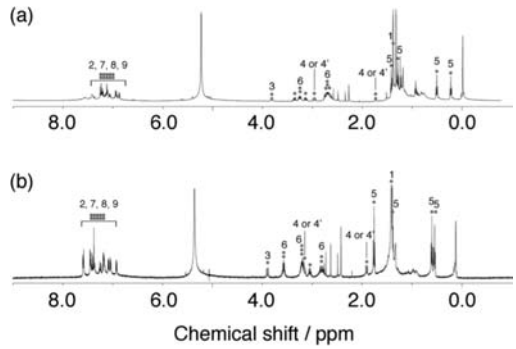

Figure 3. 500 MHz ^{1}H NMR spectra of (a) (±)-**2-A** and (b) (±)-**2-B** recorded at 293 K in CS_2/CD_2Cl_2 (1:1).

the I_h-C_{80} cage (see Figure 2). In the case of 1,3-dipolar cycloaddition, two different C−C bonds are available for reaction with azomethine ylide. One is the C−C bond between pentagonal and hexagonal rings ([5,6]-junction); the other is between two hexagonal rings ([6,6]-junction). That absorption spectra are useful to characterize the electronic structure of endohedral metallofullerenes is well-known; they are mainly attributable to $\pi-\pi^*$ transitions, which are characteristic of the cage symmetry. Both the absorption features of (±)-**2-A** and (±)-**2-B** resemble those of **4**. Accordingly, (±)-**2-A** and (±)-**2-B** are assigned as [5,6]-monoadducts, which are C_1 symmetric.

Subsequent NMR spectral examination confirmed the formation of silacyclopentane rings on the fullerene surfaces in (±)-**2-A** and (±)-**2-B**. Figure 3 shows ^{1}H NMR spectra of (±)-**2-A** and (±)-**2-B**. Numbering of the proton and carbon atoms is depicted in Figure 4. Four methyl proton signals corresponding to H_5 were observed at 0.35, 0.64, 1.39, and 1.53 ppm for (±)-**2-A** and 0.52, 0.58, 1.36, and 1.72 ppm for (±)-**2-B** as triplets. The difference in the chemical shifts of the methyl protons suggests that the conformational orientation of the Dep groups in (±)-**2-A** differs from that of (±)-**2-B**. It is particularly interesting that the two methylene proton signals corresponding to H_4 and $H_{4'}$, which are in the silacyclopentane rings, were observed at 1.82 and 3.04 ppm for (±)-**2-A** and 1.87 and 3.09 ppm for (±)-**2-B** as double doublets. This finding indicates that the silacyclopentane rings in (±)-**2-A** and (±)-**2-B** have an envelope-type conformation, which implies that one methylene proton is close to the fullerene surface, although the other is distant. A ring current of the fullerene cage is inferred to affect the former protons. Methane protons corresponding to H_3 were observed at 3.90 ppm for (±)-**2-A** and 3.86 ppm for (±)-**2-B**. The other proton signals were also assigned, supporting the fact

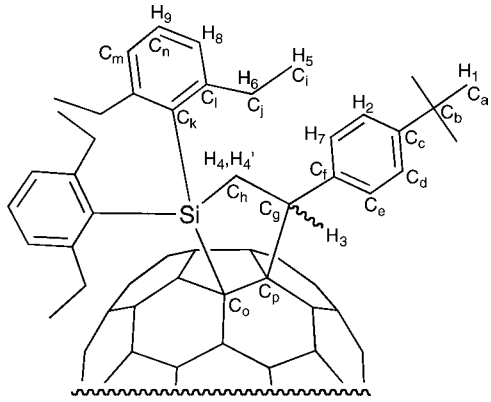

Figure 4. Numbering of protons (H_1−H_9) and carbon atoms (C_a−C_p) of (±)-**2**.

that (±)-**2-A** and (±)-**2-B** are the carbosilylated adducts. The ^{13}C NMR spectra of (±)-**2-A** shows 80 signals for the I_h-C_{80} cage, of which 78 signals are at the sp^2 carbon region of 120−160 ppm, and the other two signals at 63.84 and 64.48 ppm. Apparently, the latter are assignable to the sp^3 carbon atoms on the I_h-C_{80} cage. Similarly, the ^{13}C NMR spectra of (±)-**2-B** show that 71 out of 80 signals are at the sp^2 carbon region of 120−160 ppm. The other two signals are at 62.99 and 66.14 ppm. Accordingly, (±)-**2-A** and (±)-**2-B** are C_1 symmetric.

The detailed structure of (±)-**2-A** was revealed by single-crystal X-ray structure analysis. The crystal structure shown in Figure 5 confirms that the addition took place at the [5,6]-bond. The yielding silacyclopentane ring is in an envelope conformation, which shows good agreement with the NMR data. The Si−C bond between the addend and the fullerene cage was found to be 1.982 Å, which is around 0.13 Å longer than regular single bonds between sp^2 hybridized carbon atoms and tetracoordinated silicon.[29] This elongation is inferred as caused not only by the steric repulsion but also by the electron-donating character from the Si−C single bond orbital to π-orbitals of the vicinal carbon atoms of the cage. Similar elongation of Si−C bonds is also found in bis-silylated derivative (±)-**3**. The donating character of the silicon substituent is also confirmed using electrochemical measurements, as described later.

Table 1. La−La Atom Distances (in Å) and Site Occupancy Factors (SOFs) Determined Using Single-Crystal X-ray Crystallographic Analysis

compd	La site	La−La distance [Å]	SOF
(±)-**2-A**	La1, La2	3.796	0.639
	La3, La4	3.795	0.151
	La5, La6	3.806	0.113
	La7, La8	3.833	0.097
(±)-**3**[a]		3.792	
5[b]		3.823	

[a] Data from ref 11. [b] Data from ref 14c.

Disorder involving the La atom locations is apparent in the cage interior. As presented in Table 1, there are eight La atom sites composed of four La pairs with site occupation factors (SOFs) ranging from 0.097 to 0.639 at 90 K. The La−La distances, ranging from 3.795−3.833 Å, resemble those of (±)-**3** and **5**. This finding confirms that four La pairs exist inside the X-ray structure cage. The presence of eight La sites shows small energy differences between various orientations of the La atoms, which allow the La atoms to move around inside the cage. Additionally, it is of interest that all the La sites are positioned along a band of 10 contiguous hexagons inside the cage. Therefore, it is speculated that the circuit along the band of 10 contiguous hexagons is the predominant trajectory of the movement of La atoms, as found in the case of Ce atoms in $Ce_2@D_{5h}$-C_{80}.[30]

Variable-temperature (VT) ^{139}La NMR spectra provide information related to the dynamic behavior of the La atoms in the carbosilylated cage. For the pristine $La_2@I_h$-C_{80}, the encaged La atoms exhibit three-dimensional random movement in the icosahedral carbon sphere. The circuit of two La^{3+} cations produces a magnetic field at the La positions. This is expected to be reflected in the nuclear magnetic relaxation rate and

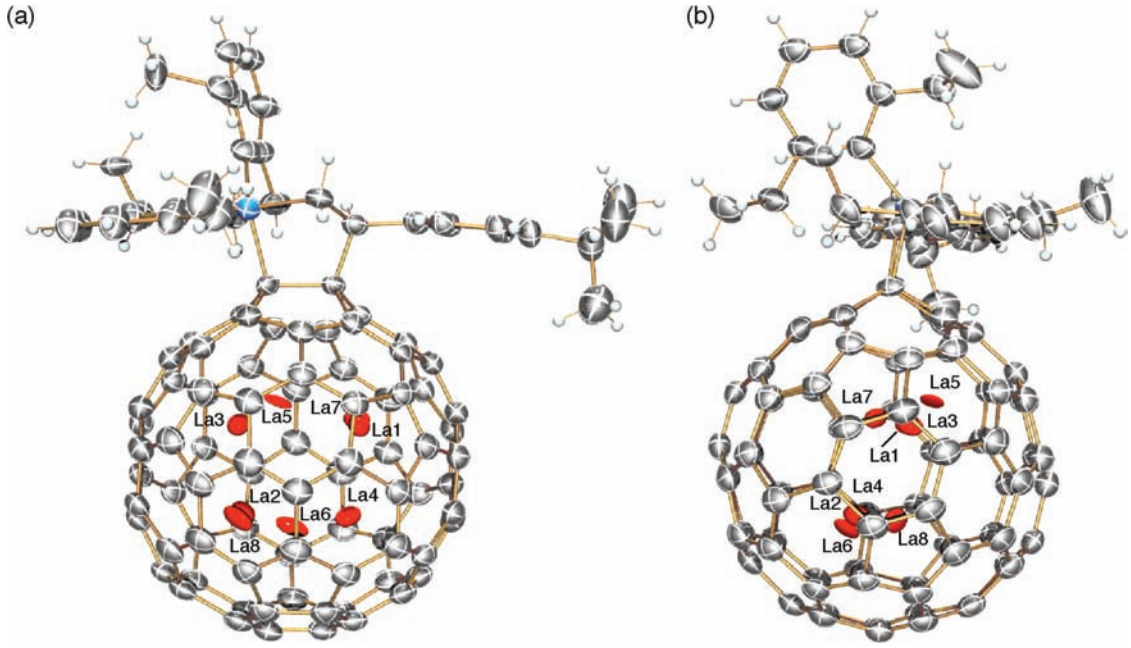

Figure 5. (a) Front and (b) left-side views of the ORTEP plot of (±)-**2-A** with thermal ellipsoids at 90 K shown at the 30% probability level. Solvate molecules are omitted for clarity.

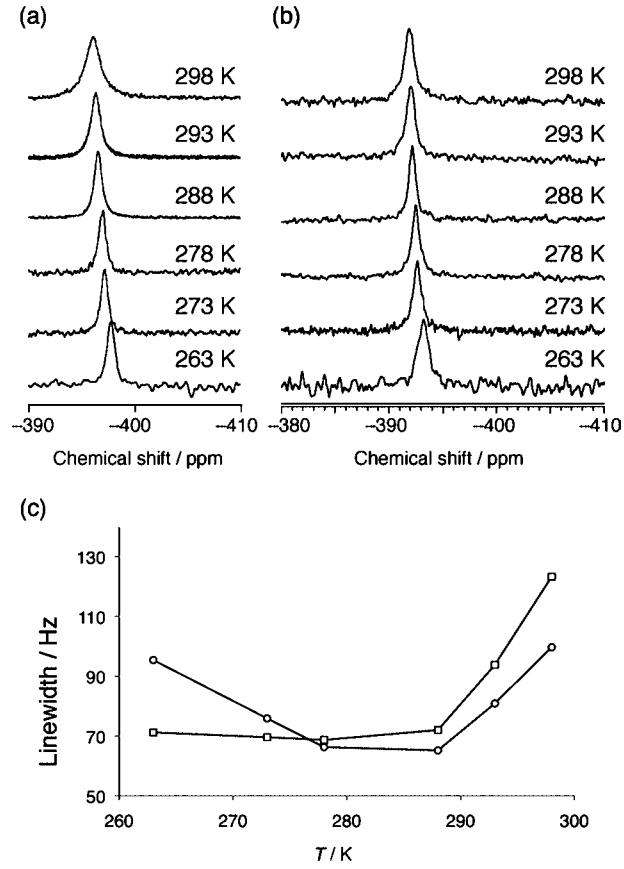

Figure 6. ^{139}La NMR spectra of (a) (±)-**2-A** and (b) (±)-**2-B** at 263−298 K, and (c) line widths of the ^{139}La signals of (±)-**2-A** (□) and (±)-**2-B** (○) as a function of temperature.

therefore the line width. Normally, the interaction between nuclear spins and the induced magnetic field (a spin-rotation relaxation) does not contribute greatly to the relaxation time in solution because neighbors dominantly quench the molecular rotation. However, the rotation of the La atoms can be preserved because of unique cage protection, so that the spin-rotation interaction has a drastic effect on the relaxation process, leading to increased line width with increasing temperature. In fact, a large broadening of the ^{139}La NMR line width with increasing temperature was observed for $La_2@I_h$-C_{80}.[31] Results of our recent study showed that the La atoms exhibit a two-dimensional hopping motion in (±)-**3**; however, the metal atoms' movement is restricted more tightly in the pyrrolidino derivatives **4** and **5**, and an adamantylidene carbene adduct, [6,6]-$La_2@I_h$-C_{80}(Ad) (**6**), in which broadening of the line width was not observed. In contrast, certain broadening phenomena were observed clearly in (±)-**2-A** and (±)-**2-B** at temperatures higher than 280 K, as shown in Figure 6. Additionally, it is noteworthy that two La atoms are equivalent at the NMR time scale. Those results demonstrate that the encaged La atoms in the carbosilylated C_{80} are not still, as in the case of **4**, **5**, and **6**. Instead, dynamic movement is apparent in (±)-**2-A** and (±)-**2-B**, as found in the X-ray structure of (±)-**2-A**. Therefore, it is concluded that the La atoms exhibit dynamic movement in the carbosilylated $La_2@I_h$-C_{80}, not only in a crystalline state but also in solution.

Theoretical Calculations. To gain deeper insight into the molecular configurations and conformations, density functional theory (DFT) calculations were conducted. Optimized structures of (±)-**2-A** and (±)-**2-B** are shown, respectively, in Figures 7 and 8. The relative energies are presented in Table 2. Because of the existence of three bulky groups that can undergo a hindered rotation, the silacyclopropane ring can form envelope-type conformation of two kinds. One conformation has a methylene moiety above the pentagon ring of the carbon cage; the other has the methylene moiety above the hexagon ring. The X-ray structure of (±)-**2-A** corresponds to **A-I**. Apparently, **A-I** is the most stable structure, in which location of the metal atoms closely resembles the La sites with the highest SOFs (i.e., La1 and La2) in the X-ray structure. Structure **A-II**, in which the La atom below the silicon atom is near, is 5.89 kcal mol^{-1} higher in energy than **A-I**. Flipping of the envelope-conformation of the silacyclopentane ring in **A-I** gives structure **A-III**, which is 9.68 kcal mol^{-1} higher in energy than that of **A-I**. Moving the La atoms in **A-III** allows structures **A-IV** and **A-V**, which are, respectively, 4.13 and 4.48 kcal mol^{-1} higher in energy than **A-III**. Therefore, changing the metal atom positions in the fullerene cage allows a smaller difference in energy than flipping the silacyclopentane ring. These results show good agreement with observation of the multiple La sites in the X-ray structure. As for (±)-**2-B**, the most stable structure is **B-IV**, in which the methylene moiety in the silacyclopentane ring is above the hexagon ring of the carbon cage. Changing the La sites gives structures **B-III** and **B-V**, which have, respectively, 3.34 and 0.96 kcal mol^{-1} higher energy than **B-IV**. However, flipping the silacyclopentane ring in **B-IV** gives **B-I**, which is 7.58 kcal mol^{-1} higher in energy than **B-IV**. Changing the La sites in **B-I** gives **B-II**, which is 0.85 kcal mol^{-1} higher in energy than **B-I**. The small difference in relative energies of the possible structures underscores that the encaged La atoms in (±)-**2-A** and (±)-**2-B** have dynamic movement inside the carbosilylated fullerene cages. It is also noteworthy that the La−La distance does not vary with the structure, which suggests that the fullerene cage was distorted only slightly by carbosilylation.

Electronic Properties. The redox potentials of (±)-**2-A** and (±)-**2-B** were investigated using cyclic (CV) and differential pulse voltammetry (DPV) measurements. The carbosilylated derivatives (±)-**2-A** and (±)-**2-B** exhibited one reversible reduction and one irreversible oxidation processes (see Figure S5 in the Supporting Information). The first oxidation of the carbosilylated derivatives led to removal of the substituents from the carbon cage. Meanwhile, (±)-**2-A** and (±)-**2-B** are stable at the first reduction potentials. Table 3 shows that the first oxidation and reduction potentials of (±)-**2-A** were shifted cathodically to 450 and 210 mV. Similarly, those of (±)-**2-B** were shifted cathodically to 430 and 180 mV. Apparently, the difference in the configuration of the tBp group does not markedly affect the electronic properties. The redox data show that the carbosilylated fullerene cage is more electron-negative than pristine $La_2@I_h$-C_{80}, indicating that the carbosilyl addend has good electron-donating character. It is noteworthy that the cathodic shifts of the reduction potentials for (±)-**2-A** and (±)-**2-B** are approximately one-half of that for (±)-**3**. In this context, carbosilylation is able to tune the electronic properties of endohedral metallofullerenes "mildly" as compared to bis-silylation. In addition, the oxidation potentials of (±)-**2-A** and (±)-**2-B** are in the

(29) Kaftory, M.; Kapon, M.; Botoshansky, M. In *The Chemistry of Organic Silicon Compounds*; Rappoport, Z., Apeloig, Y., Eds.; Wiley: New York, 1998; Vol. 2, Chapter 5.
(30) Yamada, M.; Mizorogi, N.; Tsuchiya, T.; Akasaka, T.; Nagase, S. *Chem.-Eur. J.* **2009**, *15*, 9486–9493.
(31) Akasaka, T.; Nagase, S.; Kobayashi, K.; Waelchli, M.; Yamamoto, K.; Funasaka, H.; Kako, M.; Hoshino, T.; Erata, T. *Angew. Chem., Int. Ed. Engl.* **1997**, *36*, 1643–1645.

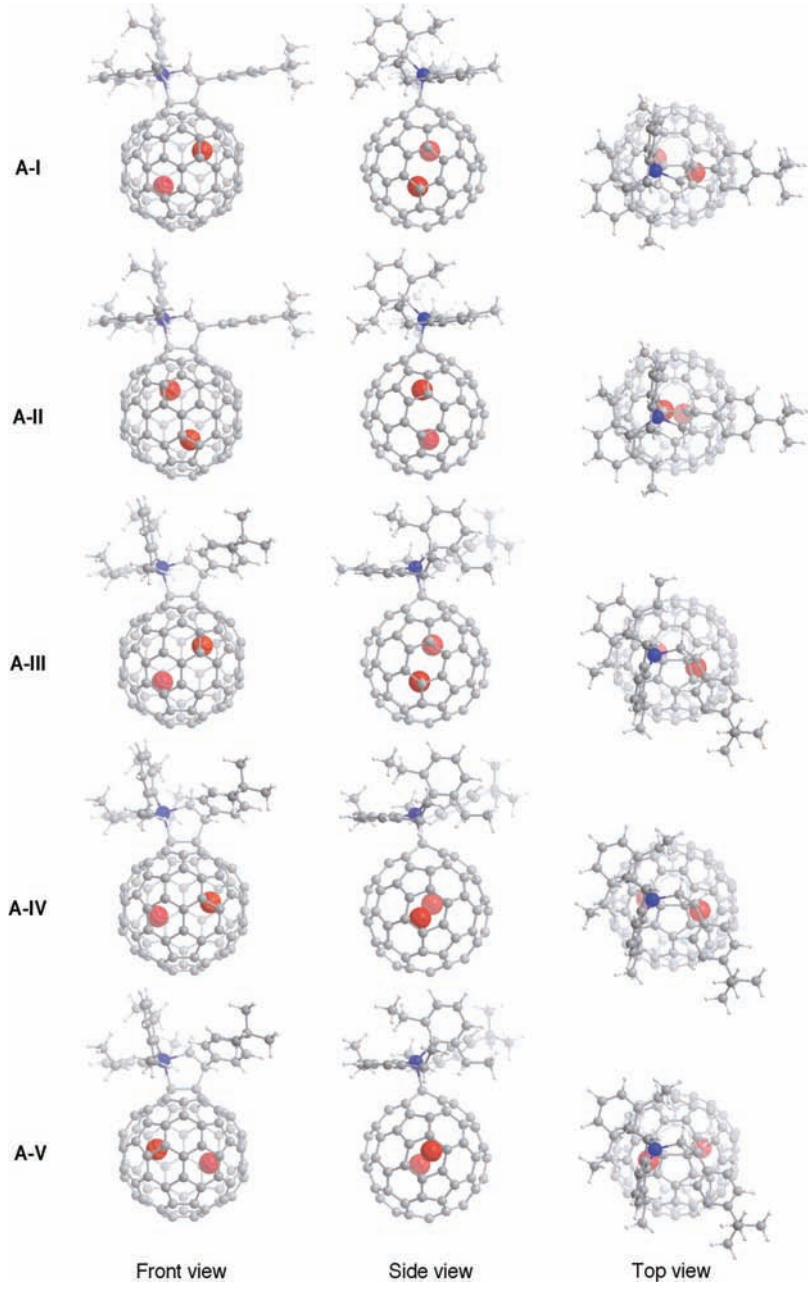

Figure 7. Optimized structures of (±)-**2-A** at the B3LYP/6-31G*∼dz level.

Table 2. Ground-State Relative Energies Computed at the B3LYP/6-31G*∼dz Level for the Optimized Structures of **2-A** and **2-B**

compd	structure	La−La distance [Å]	relative energy [kcal/mol]
(±)-**2-A**	**A-I**	3.711	0.0
	A-II	3.690	5.89
	A-III	3.710	9.68
	A-IV	3.717	13.81
	A-V	3.717	14.16
(±)-**2-B**	**B-I**	3.711	8.25
	B-II	3.709	9.10
	B-III	3.717	4.01
	B-IV	3.711	0.67
	B-V	3.710	1.63

range of the oxidation potential of $La_2@I_h$-C_{80} and that of (±)-**3**. Therefore, it is concluded that the electronic properties of endohedral metallofullerenes can be modulated step-by-step by the number of silicon atoms introduced on the cage.

Conclusions

We have described thermal carbosilylation of endohedral dimetallofullerene $La_2@I_h$-C_{80} with proper silirane for the first time. Two diastereomers of the carbosilylated adducts were isolated and characterized using NMR spectroscopy and X-ray crystallographic analysis. In particular, crystallographic analysis of (±)-**2-A** revealed that addition of silirane took place at the [5,6]-bond, yielding formation of silacyclopentane rings on the C_{80} cage. Single-crystal X-ray crystallographic and ^{139}La NMR spectral analyses revealed that the encaged La atoms in the

(32) Suzuki, T.; Maruyama, Y.; Kato, T.; Kikuchi, K.; Nakao, Y.; Achiba, Y.; Kobayashi, K.; Nagase, S. *Angew. Chem., Int. Ed. Engl.* **1995**, *34*, 1094–1096.

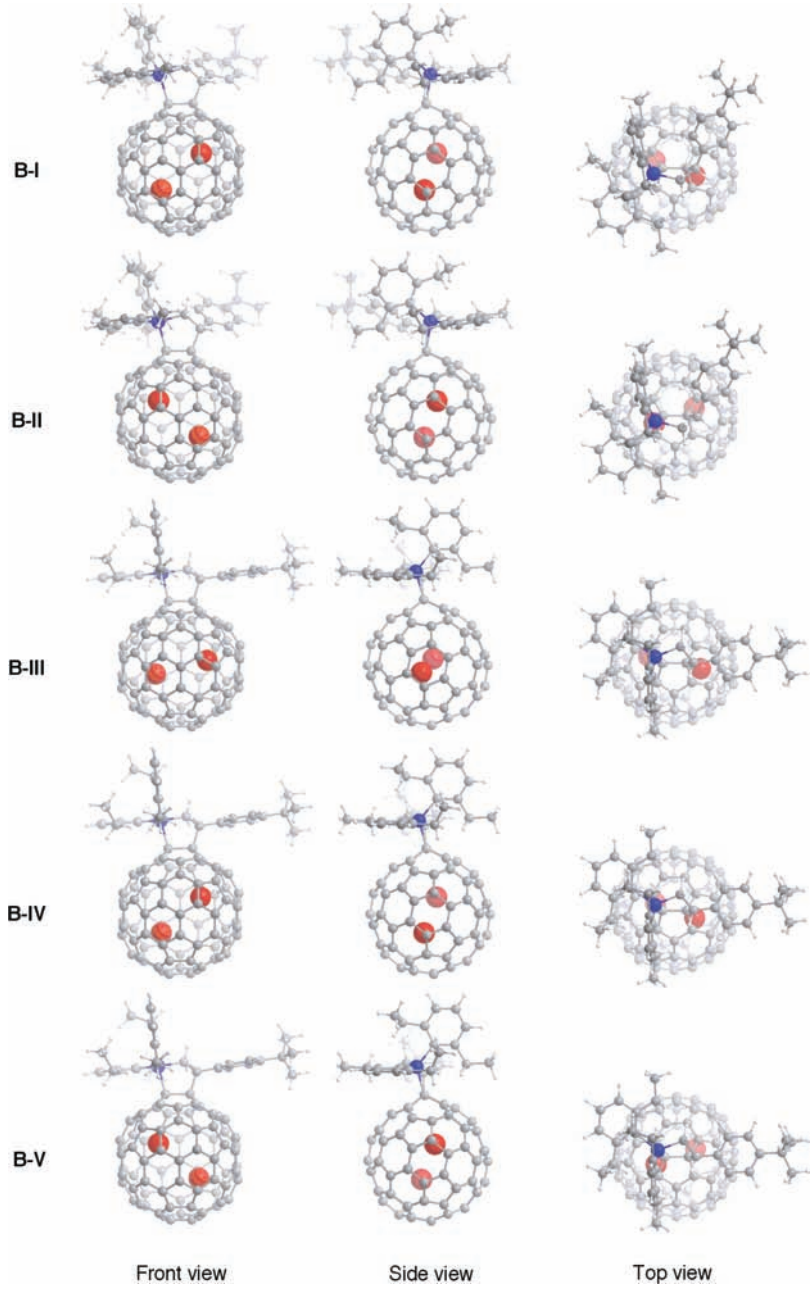

Figure 8. Optimized structures of (±)-**2-B** at the B3LYP/6-31G*∼dz level.

Table 3. Redox Potentials[a] of (±)-**2-A**, (±)-**2-B**, (±)-**3**, and $La_2@I_h$-C_{80}

compd	$^1E_{ox}$	$^1E_{red}$
(±)-**2-A**	+0.11[b]	−0.50
(±)-**2-B**	+0.13[b]	−0.53
(±)-**3**[c]	−0.04[b]	−0.70
$La_2@I_h$-C_{80}[d]	+0.56	−0.31

[a] Values are given in volts and are relative to ferrocene/ferrocenium couple and were obtained by DPV. [b] Irreversible. [c] Data from ref 11. [d] Data from ref 32.

carbosilylated derivatives show dynamic motion, which is supported by DFT calculations. Electrochemical measurements disclosed that introduction of silicon atoms onto the fullerene surface mildly changes the electronic properties of endohedral metallofullerenes. Results of this study underscore that the number of silyl groups placed onto the fullerene surfaces plays an important role in alternation of electronic properties and metal atoms' movement. These results open up a new avenue of silicon−carbon−metal hybrids.

Acknowledgment. M.Y. thanks the Japan Society for the Promotion of Science (JSPS) for a Research Fellowship for Young Scientists. This work was supported in part by a Grant-in-Aid for Scientific Research on Innovative Areas (No. 20108001, "pi-Space") from the Ministry of Education, Culture, Sports, Science, and Technology of Japan.

Supporting Information Available: Complete ref 26, spectroscopic data, crystallographic data in CIF format, and theoretical results for the carbosilylated adducts. This material is available free of charge via the Internet at http://pubs.acs.org.

JA108671B